Journal of Thermal Analysis and Calorimetry
https://doi.org/10.1007/s10973-024-13844-8

Polymorphic crystallization and transformation pathways of 1,2-dipalmitoyl-3-oleoyl-*rac*-glycerol (PPO) during a liquid–solid-liquid journey

Jorge Macridachis[1] · Laura Bayés-García[1] · Teresa Calvet[1]

Received: 29 November 2023 / Accepted: 7 November 2024

Abstract
The polymorphic behavior of triacylglycerol (TAG) crystals formed during the manufacturing process of lipid-based food products relates directly to their textural and melting properties. In this work, we analyzed the polymorphic crystallization and transformation behavior of 1,2-dipalmitoyl-3-oleoyl-*rac*-glycerol (PPO), a widespread TAG in edible fats and oils, during the application dynamic thermal treatments of cooling and heating. By implementing calorimetric, *X*-ray diffraction, and microscopy techniques, we mapped the polymorphic occurrence and the polymorphic transformation pathways of PPO as a function of the rate of thermal treatments. The results obtained were later compared to that reported for diverse TAGs in previous studies. Despite the overall crystallization and transformation behavior of PPO following a similar trend to other TAGs close in fatty acid composition, we can highlight the much lower influence of varying cooling and heating conditions on the crystallization properties of this TAG. In more detail, crystalline forms of low stability were generally promoted during crystallization, whereas transformations occurred always through the melt independently of the heating conditions. One may expect this behavior to influence the industrial processing and final properties of food products based on edible fats containing PPO.

Keywords Crystallization · Polymorphism · Thermal analysis · Triacylglycerol · *X*-ray diffraction · Thermal treatment

Introduction

Molecular crystals contained in lipid-based food products relate directly to properties such as texture, melting behavior, flavor and oil loss. More specifically, and despite the presence of further lipidic components, these characteristics primarily depend on the crystals formed by triacylglycerols (TAGs) within the fats and oils used in their formulation. Since the sensory properties and shelf-life of foods dictate whether or not a food product is accepted by consumers, understanding the crystallization behavior of TAGs has become essential for food producers.

During crystallization, TAGs molecules, which consist of three esterified fatty acid moieties in a glycerol backbone, pack laterally forming repetitive lamellar structures which constitute the whole crystal network. The crystallization and polymorphic behavior of TAGs forming natural products strongly depend on the fatty acid components type, which mainly include saturated straight and/or bent cis-unsaturated fatty acid chains. According to the cross-sectional packing mode of TAGs and the resulting subcell structure, three main polymorphs are usually formed, namely α, β', and β, which exhibit a hexagonal, orthorhombic perpendicular, and triclinic parallel subcell, respectively [1]. Thus, β crystals contribute to the brightness and snap of chocolate, whereas the texture of spreads is achieved by promoting the development of β' crystals [2, 3]. According to the number of fatty acid chains or leaflets forming the long-chain axis of lamellar structures, polymorphs usually present a double (2L) or a triple (3L) chain-length structure.

Given the importance of TAG polymorphism in food manufacturing, many studies on lipids and TAGs crystallization have taken into consideration industry-related external factors to which food products may be exposed (e.g. shear, sonication, or thermal treatments). For instance, Mazzanti

✉ Laura Bayés-García
laurabayes@ub.edu

[1] Departament de Mineralogia, Petrologia i Geologia Aplicada, Facultat de Ciències de la Terra, Universitat de Barcelona, Martí i Franquès s/n, 08028 Barcelona, Spain

Published online: 26 November 2024

et al. demonstrated, through the α and β' forms of milk fat and palm oil, that shear may accelerate polymorphic transitions [4]. This behavior was ascribed to the energy provided by shear to induce solid-state or melt-mediated transitions. In line with these, extensive work has been carried out to address the suitability of the technique to induce the occurrence of βv form of cocoa butter for chocolate production [5, 6]. Regarding sonication procedures, high-intensity ultrasound treatments have shown significant potential for modulating crystal sizes, hardness and polymorphic transitions in complex fats [7, 8], but also in single TAG components. As an example, sonication has been demonstrated as a powerful tool for controlling the β crystallization of fully saturated molecules [9]. Finally, crystallization studies of lipid systems, and specially, pure TAGs under the influence of tailored thermal treatments have allowed to shed light into their polymorphic crystallization and transformation mechanisms. In this sense, the isothermal crystallization behavior of 1,2,3-tripalmitoyl glycerol (PPP, with P being a saturated palmitic acid) at varying temperatures showed increasing induction times for the occurrence of α, β', and β crystals [10]. A later work on 1,3-dipalmitoyl-2-oleoyl glycerol (POP) and 1,3-distearoyl-2-oleoyl glycerol (SOS, with S and O being saturated stearic and monounsaturated oleic acid, respectively), arrived at the same conclusion and demonstrated a higher crystallization rate of TAGs via melt-mediated transition as compared to melt-cooling at the same crystallization temperature [11]. Polymorphic studies performed on diverse saturated–unsaturated mixed-acid TAGs containing palmitic/stearic and oleic fatty acid moieties, such as 1-palmitoyl-2,3-dioleoyl-*rac*-glycerol (POO), 1-stearoyl-2,3-dioleoyl-*rac*-glycerol (SOO), 1,3-dioleoyl-2-palmitoyl glycerol (OPO), 1,3-dioleoyl-2-stearoyl glycerol (OSO), 1,3-dipalmitoyl-2-oleoyl glycerol (POP), or 1,3-distearoyl-2-oleoyl glycerol (SOS) cooled and reheated at varying rates provided information of practical value regarding the kinetic influence on the crystalline behavior of pure components as follows: (i) specific polymorphic forms can be targeted during melt-crystallization processes by controlling the speed of cooling; (ii) during polymorphic transformations, the occurrence or not of some metastable phases largely depends on the heating rate applied; and (iii) polymorphic transformation pathways (melt-mediation, solid-state transformations, or via kinetic liquid crystal occurrence) can be controlled through the speed of heating [12–15].

The overall behavior of TAGs under the effects of dynamic thermal treatments has been largely stablished by the former studies. However, these also showed that the extent of this influence also relies on intrinsic properties of TAGs, such as molecular symmetry or fatty acid composition. As an example, the favored solid-state transformations described for POO as compared to POP when heating at the same rates was ascribed to a higher oleic acid content [11, 15]. This evidences that to fully understand complex lipid systems, further work still needs to be done to unveil the differences between individual TAG species.

To the best of our knowledge, no detailed studies on the polymorphic crystallization and transformation behavior of asymmetric highly-saturated TAGs based on palmitic and oleic acids have been described to date. In order to go further on this matter, we used differential scanning calorimetry (DSC), laboratory-scale and synchrotron radiation (SR) *X*-ray diffraction (XRD) techniques to analyze the polymorphic occurrence and transformation routes of 1,2-dipalmitoyl-3-oleoyl-*rac*-glycerol (PPO), which becomes a major component in semi-solid fats such as lard or palm oil [16], and exerts a relevant role on the crystalline behavior of olive oil solid fractions [17]. In addition, according to previous work, PPO exhibits metastable α_2-2L, α_1-3L, and β'_2-2L forms and a stable β'_1-3L form [18], which makes lipids and fractions rich in this TAG of special interest for the development of shortenings, spreadable products, and confections. Aiming to emulate real industrial operation conditions, in the present work the polymorphic behavior of this TAG was investigated when subjected to thermal treatments of cooling and subsequent heating at rates ranging from low (0.5 °C min^{-1}) to very high (15 °C min^{-1}) rates. The properties exhibited by PPO during the study were then analyzed and compared to that of saturated–unsaturated mixed-acid TAGs exhibiting varying fatty acid composition, molecular distribution and degree of unsaturation.

Materials and methods

Materials

1,2-Dipalmitoyl-3-oleoyl-*rac*-glycerol (PPO) of purity > 99% was purchased from Larodan AB (Solna, Sweeden) and used as received.

Differential scanning calorimetry (DSC)

Thermal analyses were conducted on a PerkinElmer DSC-Diamond calorimeter working at atmospheric pressure and under a nitrogen flow of 20 cm^3 min^{-1}. The calibration of the equipment was carried out using the melting temperature and enthalpy data of indium and n-decane standards when heated at 2 °C min^{-1}. 4–4.4 mg of sample were placed into 50 µL aluminum pans and hermetically sealed. An empty pan was used as a reference. DSC curves were processed with Pyris software to obtain the onset, peak top, and end temperatures (T_{onset}, T_{top}, and T_{end}, respectively), and enthalpy (ΔH) of the thermal events registered. Unless otherwise indicated, T_{onset} will be used to define the temperature of the thermal events detected by DSC.

Molten PPO samples kept at 50 °C for several minutes were first cooled to −80 °C min^{-1} to induce the crystallization and subsequently heated until complete melting at varying rates of 15, 5, 2, 0.5, or 0.1 °C min^{-1}. Three independent samples were employed for each of the thermal treatments applied. For experiments carried out at cooling and heating rates different from that used during the equipment calibration, a correction described elsewhere [19] was applied to the temperature values obtained from the integration of DSC peaks. Student's method approximation was used to estimate the random uncertainty of temperature and enthalpy values with a 95% threshold reliability.

X-ray diffraction (XRD) experiments

To identify the polymorphic forms occurring during the crystallization and transformation events detected by DSC, the same thermal protocols were applied during laboratory-scale and synchrotron radiation *X*-ray diffraction (lab-scale XRD and SR-XRD, respectively) measurements. SR-XRD was used to analyze the samples subjected to faster cooling/heating treatments (15, 5, and 2 °C min^{-1}), whereas lab-scale XRD was generally employed in experiments based on lower rates (0.5 and 0.1 °C min^{-1}).

The SR-XRD study of the samples was done at beamline BL11-NCD-SWEET of the ALBA Synchrotron facility (Cerdanyola del Vallès, Barcelona, Spain) using a wavelength, λ, of ~ 0.1 nm (12.4 keV). A Pilatus 1 M detector (pixel size of 172 µm X 172 µm) and a LX255-HS Rayonix detector (pixel size of 44 mm X 44 mm) were used to record SAXD and WAXD data, respectively. Silver behenate was used to calibrate q-axis of SR-SAXD patterns, whereas Cr_2O_3 was employed for SR-WAXD patterns. The temperature of the sample (2 mm thick), contained in an aluminum cell sealed with kaptom film windows, was controlled by a Linkam stage. SR-SAXD and SR-WAXD patterns were taken simultaneously at 20 s or 30 s intervals, depending on the rate of the thermal treatments (cooling/heating) applied. The software pyFAI was used to integrate the 2D SR-WAXD into the 1D data. SR-SAXD data were processed with in-house software, whereas Igor Pro V6.3.7.2 was used for data analysis.

Lab-scale XRD measurements were carried out on a PANalytical X'Pert Pro MPD powder diffractometer with the Debye–Scherrer Geometry and equipped with a hybrid monochromator and a PIXcel detector. During cooling and heating treatments, the temperature was controlled through an Oxford Cryostream Plus 220 V. To avoid preferential crystalline orientation, the 1 mm diameter Lindemann glass capillary containing the sample was rotated around its axis throughout the analysis. Lab-scale XRD data was acquired in the 2θ range from 1° to 28° with a step size of 0.013° and a measuring time of 150 s. X'Pert Highscore V2.2e software was used for data analysis.

Thermo-optical polarized light microscopy (TOPLM)

The microscopic study of samples subjected to the same thermal protocols described above was carried out by using a Nikon Eclipse 50iPol Microscope. The same was equipped with a Linkam THMSG-600 stage coupled to an LNP liquid nitrogen cooling system and a TMS94 temperature controller. A Nikon Digital Camera DXM1200F was used to capture images of the sample at different time intervals, which were then processed by Linksys software. For microscopic analyses, two independent samples were prepared by pipetting 1.5 µL of molten PPO into a glass slide, after which a coverslip was carefully placed on the top to avoid the presence of air.

Results

DSC, XRD and TOPLM techniques were combined to monitor the polymorphic crystallization, transformation and melting behavior of PPO when cooled from the melt to −80 °C and subsequently heated at different rates of 0.1, 0.5, 2, 5, and 15 °C min^{-1}. Complete DSC data regarding temperatures and enthalpy values associated to the thermal phenomena observed are summarized in Tables S1 and S2 of supplementary material. Diffraction data of polymorphic forms of PPO, those determined in the present work and those obtained from previous literature, which were used as a reference, are shown in Table 1.

Table 1 Long and short spacing values of PPO polymorphic forms detected in the present (A) and previous work (B) (Mizobe et al., 2013)

		sub-α_2-2L	sub-α_1-3L	α_2-2L	α_1-3L	β'_2-2L	β'_1-3L
A	Long spacing/nm	4.1	3.9	4.9 → 4.1	7.6 (3.9)	4.2	6.4 (3.2)
	Short Spacing/nm	0.42,0.38	0.42, 0.38	0.41	0.41	0.42, 0.39	0.42, 0.38
B	Long spacing/nm	–	–	4.98 → 3.92	7.8	4.2	6.7
	Short Spacing/nm	–	–	0.41	0.41	0.41, 0.38	0.41, 0.38

→ denotes a change in lamellar organization of the initially formed crystals

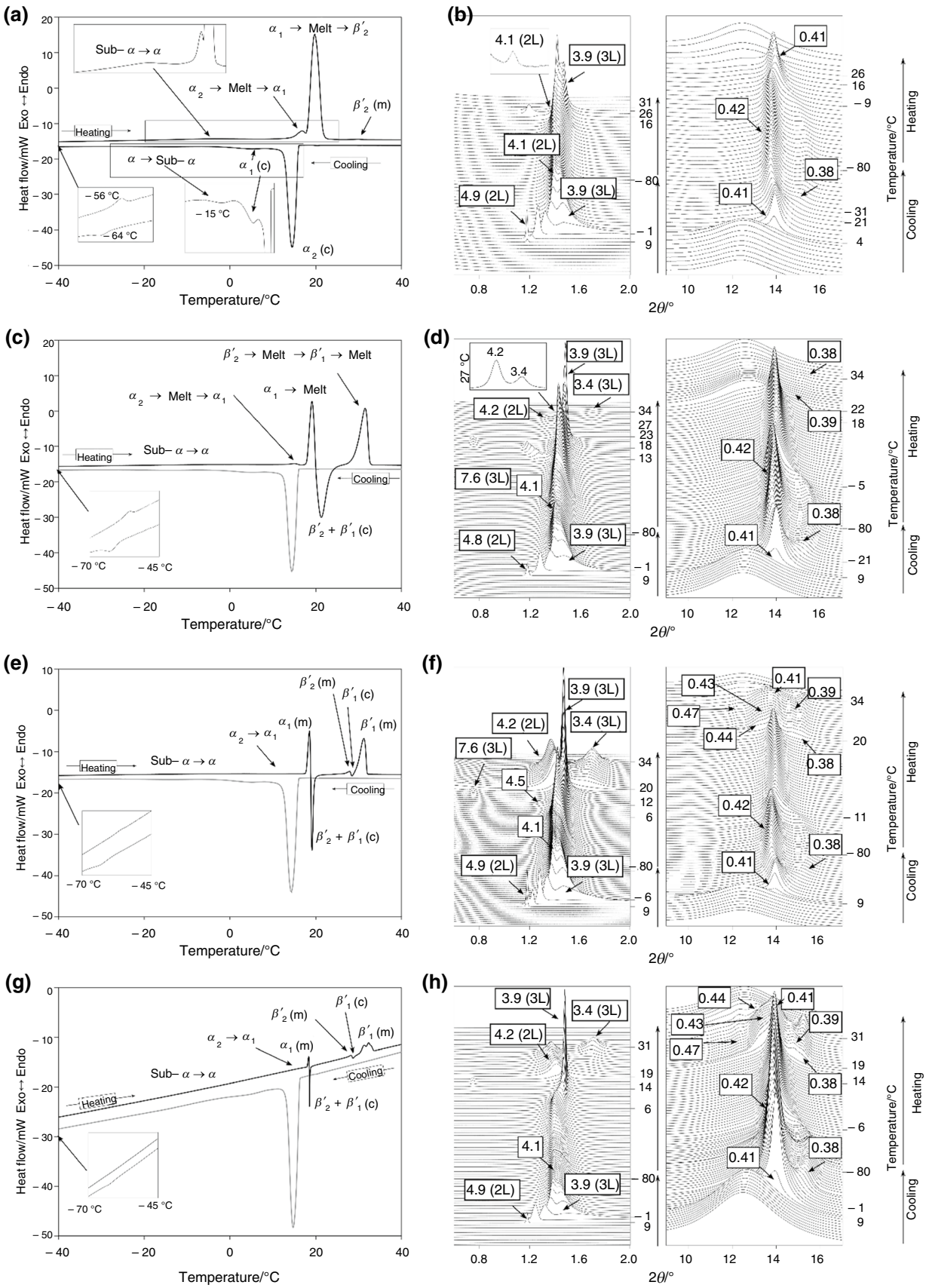
(a)
Heat flow/mW Exo ↔ Endo
Temperature/°C
Sub– α → α
α1 → Melt → β′2
α2 → Melt → α1
β′2 (m)
Heating
α → Sub– α
α1 (c)
Cooling
– 56 °C
– 64 °C
– 15 °C
α2 (c)
(b)
4.1 (2L)
3.9 (3L)
0.41
0.42
4.1 (2L)
0.38
4.9 (2L)
3.9 (3L)
0.41
Temperature/°C
Heating
Cooling
2θ/°
(c)
Heat flow/mW Exo ↔ Endo
Temperature/°C
β′2 → Melt → β′1 → Melt
α2 → Melt → α1
α1 → Melt
Heating
Sub– α → α
Cooling
β′2 + β′1 (c)
– 70 °C
– 45 °C
(d)
27 °C
4.2
3.4
3.9 (3L)
3.4 (3L)
4.2 (2L)
0.38
0.39
0.42
7.6 (3L)
4.1
0.38
4.8 (2L)
3.9 (3L)
0.41
Temperature/°C
Heating
Cooling
2θ/°
(e)
Heat flow/mW Exo ↔ Endo
Temperature/°C
β′2 (m)
β′1 (c)
α2 → α1
α1 (m)
β′1 (m)
Heating
Sub– α → α
Cooling
β′2 + β′1 (c)
– 70 °C
– 45 °C
(f)
3.9 (3L)
0.43
0.41
0.39
0.47
4.2 (2L)
3.4 (3L)
0.44
7.6 (3L)
0.38
4.5
0.42
4.1
0.38
4.9 (2L)
3.9 (3L)
0.41
Temperature/°C
Heating
Cooling
2θ/°
(g)
Heat flow/mW Exo ↔ Endo
Temperature/°C
β′2 (m)
β′1 (c)
α2 → α1
α1 (m)
β′1 (m)
Sub– α → α
Cooling
Heating
β′2 + β′1 (c)
– 70 °C
– 45 °C
(h)
3.9 (3L)
3.4 (3L)
0.44
0.41
4.2 (2L)
0.43
0.39
0.47
0.42
0.38
4.1
0.41
0.38
4.9 (2L)
3.9 (3L)
Temperature/°C
Heating
Cooling
2θ/°

◂**Fig. 1** DSC curves (left) and SR-XRD patterns (right) of PPO cooled at 15 °C min^{-1} and subsequently heated at **A, B** 15 °C min^{-1}, **C, D** 5 °C min^{-1}, **E, F** 2 °C min^{-1}, and **G, H** 0.5 °C min^{-1}. (c): crystallization; (m): melting. *d*-spacing values are given in nm

DSC and XRD study

Cooling at 15 and 2 °C min^{-1} and heating at different rates

Figure 1 depicts the DSC curves and SR-XRD patterns obtained when molten PPO was cooled at 15 °C min^{-1} and reheated at fast to low rates of 15, 5, 2, and 0.5 °C min^{-1}.

During rapid cooling of PPO at 15 °C min^{-1}, three main crystallization events were detected. The first one (T_{onset} ~ 16 °C) was due to the formation of α_2-2L polymorph, as confirmed by the presence of reflections at 4.9 and 0.41 nm in SR-SAXD and SR-WAXD, respectively (see SR-XRD patterns acquired at 9 °C in Fig. 1B). The complicated molecular packing of PPO caused by steric hindrance between saturated and unsaturated acyl chains (palmitic and oleic acids) resulted in the shifting of the α_2-2L reflection at 4.9 nm to 4.1 nm at decreasing temperature. According to previous work, the formation of empty regions in the lamellar structure of TAGs including saturated and unsaturated acyl chains may allow a non-stop reorganization of α-2L crystals during cooling [20]. α_1-3L was formed during the second crystallization event (see enlarged image in Fig. 1A), according to the 3L SR-SAXD peak emerging at 3.9 nm below 9 °C. Then, a $\alpha \rightarrow$ sub-α transition occurred at about −15 °C. As a result, the typical SR-WAXD pattern of a hexagonal subcell (single reflection at 0.41 nm) became that of a pseudo-hexagonal subcell near this temperature (reflections at 0.42 and 0.38 nm). The final DSC exothermic event observed at ~ −64 °C was not identified through SR-XRD, which also was detected for PPO cooled at lower rates and may probably be due to subtle changes in the existing structures by cause of steric hindrance rather than by the occurrence of new crystalline phases. The occurrence of structural changes in PPO even at temperatures far below 0 °C may also be influenced by an asymmetric distribution of fatty acids at the *sn*- positions of the glycerol group. This would be supported by the detection of a similar low-temperature polymorphic event in SSO [12] and the absence thereof in the symmetric TAGs POP and SOS [12, 14]. α and sub-α crystals were also obtained in PPO cooled at 2 °C min^{-1} (see related experimental data in Fig. 2). However, the slower cooling rate allowed a better insight into the polymorphic development of PPO under dynamic thermal conditions.

SR-SAXD showed again the first occurrence of α_2-2L at approximately 15 °C through the reflection at 4.9 nm (DSC crystallization event at T_{onset} of ~ 17 °C). At decreasing temperature, the reflection shifted to 4.0 nm and decreased in intensity as the one of α_1-3L at 3.9 nm emerged at 12 °C and grew. Thus, α_2-2L crystals seemed to act as precursors of the initial formation of α_1-3L, which eventually became predominant in the sample. The growth of α_1-3L at the expense of α_2-2L during cooling under non-isothermal conditions, confirmed in the present work by SR-XRD, was already suggested by a previous DSC study on PPO [21]. Recently, the same has been reported for isothermally crystallized PPO [22].

When reheated at the rates of 15, 5, 2, and 0.5 °C min^{-1}, PPO samples cooled at 15 or 2 °C min^{-1} exhibited a similar sequence of polymorphic transitions. These will be described through the experimental data obtained when cooled at 15 °C min^{-1} (Fig. 1). Additional data on PPO heated at the same rates after cooling at 2 °C min^{-1} can be found in Figure S1 of supplementary information.

The sub-α to α_2-2L and α_1-3L transition of PPO when heated at 15 °C min^{-1} resulted in a single SR-WAXD reflection at 0.41 nm when reaching 9 °C (see Fig. 1B) and a small perturbation in the baseline of the DSC curve at ~ 5 °C (Fig. 1A). Several degrees above, the α_2-2L SR-SAXD peak at 4.1 nm shifted again to 4.9 nm, which confirmed the reversibility of the changes in lamellar ordering undergone by α_2-2L at the earliest stage of crystallization from the melt. Then, α_2-2L form transformed via melt-mediation into α_1-3L (see the strengthening of the reflection at 3.9 nm at the expense of that at 4.9 nm in SR-SAXD patterns) leading to the melting peak detected at ~ 14 °C by DSC. Its overlapping with the α_1-3L melting signal hampered the identification of an intermediate crystallization event. No further changes occurred in SR-WAXD patterns but the weak reflection at 4.1 nm shown by SR-SAXD patterns when reaching 26 °C suggested the last DSC peak at ~ 29 °C as the melting of β'_2-2L crystals formed from the α_1-3L melt.

Similarly, sub-$\alpha \rightarrow \alpha_2$-2L + α_1-3L and α_2-2L → melt → α_1-3L transitions were firstly identified in PPO heated at 5 °C min^{-1} (see experimental data in Fig. 1C and D). However, in this case, the DSC peak due to the melting of α_1-3L was followed by a strong crystallization event (T_{onset} ~ 20 °C; $\Delta H = -110$ J g^{-1}) before the complete melting of the sample. According to reflections at 0.39 and 0.38 nm in SR-WAXD, and 4.2 and 3.4 nm in SR-SAXD patterns above 20 °C, β'_2-2L and most stable β'_1-3L crystals were formed from the α_1-3L melt. At above 27 °C, the intensity of the β'_1-3L SR-SAXD reflection increased, and that of β'_2-2L, decreased. Thus, the final DSC peak detected at 29 °C resulted from the convolution of the melt-mediated β'_2-2L → β'_1-3L transformation and the subsequent β'_1-3L melting.

The sequence of polymorphic transformations of PPO did not vary for PPO heated at 2 or 0.5 °C min^{-1}, but reducing the heating rate had a positive impact on the amount of more stable crystalline forms occurring during transformations. In both cases, the low energy involved in the α_2-2L to α_1-3L transition hampered the identification of the corresponding

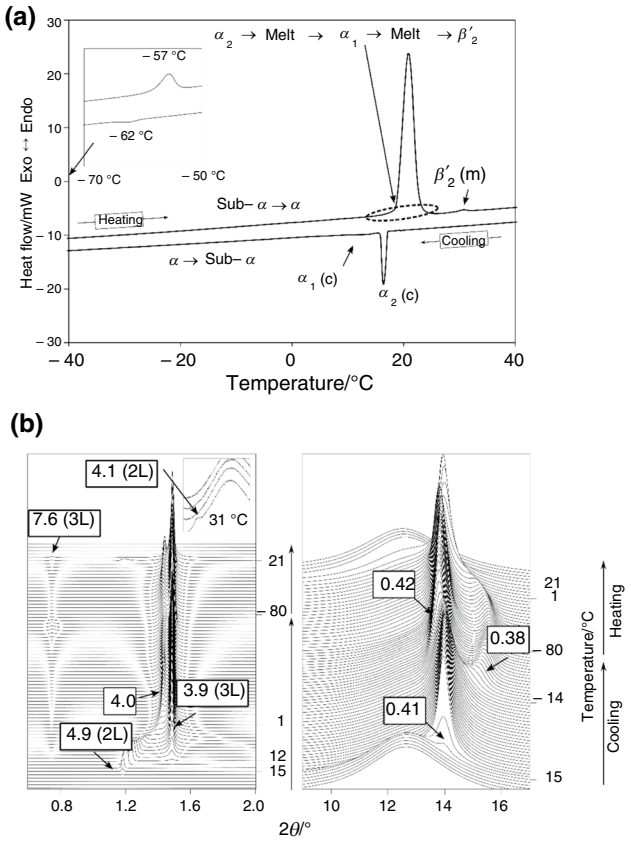

Fig. 2 DSC curves **A** and SR-XRD patterns **B** of PPO cooled at 2 °C min^{-1} and subsequently heated at 15 °C min^{-1}. (c): crystallization; (m): melting. *d*-spacing values are given in nm

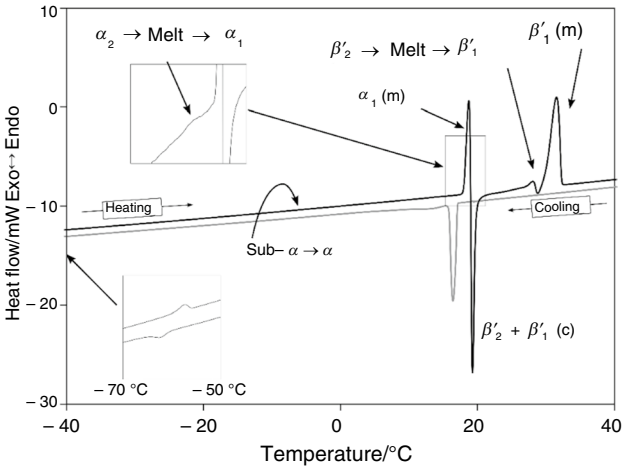

Fig. 3 DSC curves of PPO cooled and subsequently heated at 2 °C min^{-1}. (c): crystallization; (m): melting

thermal signals in the DSC curves (see Fig. 1E and G). However, the thermal data obtained for PPO cooled and reheated at 2 °C min^{-1} (Fig. 3) suggested that this transformation still takes place via melt-mediation at low heating rates.

Once α_1-3L vanished from SR-XRD patterns, SR-SAXD reflections at 4.2 and 3.4 nm were stronger than those observed when PPO was heated at 15 and 5 °C min^1 (see Fig. 1F and H). In addition, β' reflections at 0.47, 0.44, 0.43, 0.41, 0.39, and 0.38 nm were clearly discerned in the corresponding SR-WAXD patterns. Therefore, a higher amount of β'_2-2L and β'_1-3L was formed from the α_1-3L melt when cooling at low rates. This was the result of the much higher time provided for the molecular arrangement in a novel structure when reducing the speed of heating. The next melt-mediated β'_2-2L → β'_1-3L transformation and final β'_1-3L melting led to successive endothermic → exothermic → endothermic events ranging from around 27 to 33 °C (Fig. 1E and G). Due to the similar subcell characteristics of the two β' forms, the β'_2-2L to β'_1-3L transition was more easily followed through the changes in intensity of reflections at 4.2 and 3.4 nm in SR-SAXD patterns. However, the SR-WAXD peak at 0.39 nm vanished and that at 0.38 nm strengthened near 31 °C when heating at 0.5 °C min^1 (Fig. 1H). This led us to conclude that the first reflection must correspond to β'_2-2L and the second to β'_1-3L.

Cooling at 0.5 or 0.1 °C min^{-1} and heating at different rates

Lowering the cooling rate applied allowed obtaining more stable forms of PPO during crystallization. At 0.5 °C min^{-1} (see Fig. 4A and B), β'_2-2L crystallized first, according to the SR-SAXD peak at 4.1 nm and corresponding SR-WAXD signals at 0.41 and 0.39 nm noted at 18 °C. Soon after, α_2-2L (SR-SAXD peak at 4.8 nm) and α_1-3L (7.6 and 3.9 nm) were formed.

The complete vanishing of α_2-2L in SR-SAXD patterns just after its occurrence indicated a complete α_2-2L → α_1-3L transition at this cooling rate. In PPO cooled at 0.1 °C min^{-1} (Fig. 5), the single peak detected at ~ 23 °C by DSC was due to the formation of β' crystals.

Peaks at 0.44, 0.41, and 0.38 nm emerged in lab-scale WAXD patterns acquired at 20 °C, whereas peaks at 4.2 and 3.4 nm (002 reflection) belonging to β'_2-2L and β'_1-3L crystals, respectively, were identified in the SAXD region. The intensity ratio of the diffraction signals indicated that the occurrence of β'_1-3L was noticeably favored with respect to β'_2-2L.

As to the polymorphic transitions detected when heating the slowly crystallized PPO, they were consistent with those observed in samples cooled at higher rates, although subtle differences were identified. In PPO cooled at 0.5 °C min^{-1} and reheated at 15 °C min^{-1}, the sequence of transitions α_1-3L → melt → β'_2-2L → melt was more easily monitored by DSC (Fig. 4A) as compared to PPO cooled at 15 and 2 °C min^{-1} (see Figs. 1 and 2). The stronger thermal signal resulting from the melting of β'_2-2L (peak at about 28 °C)

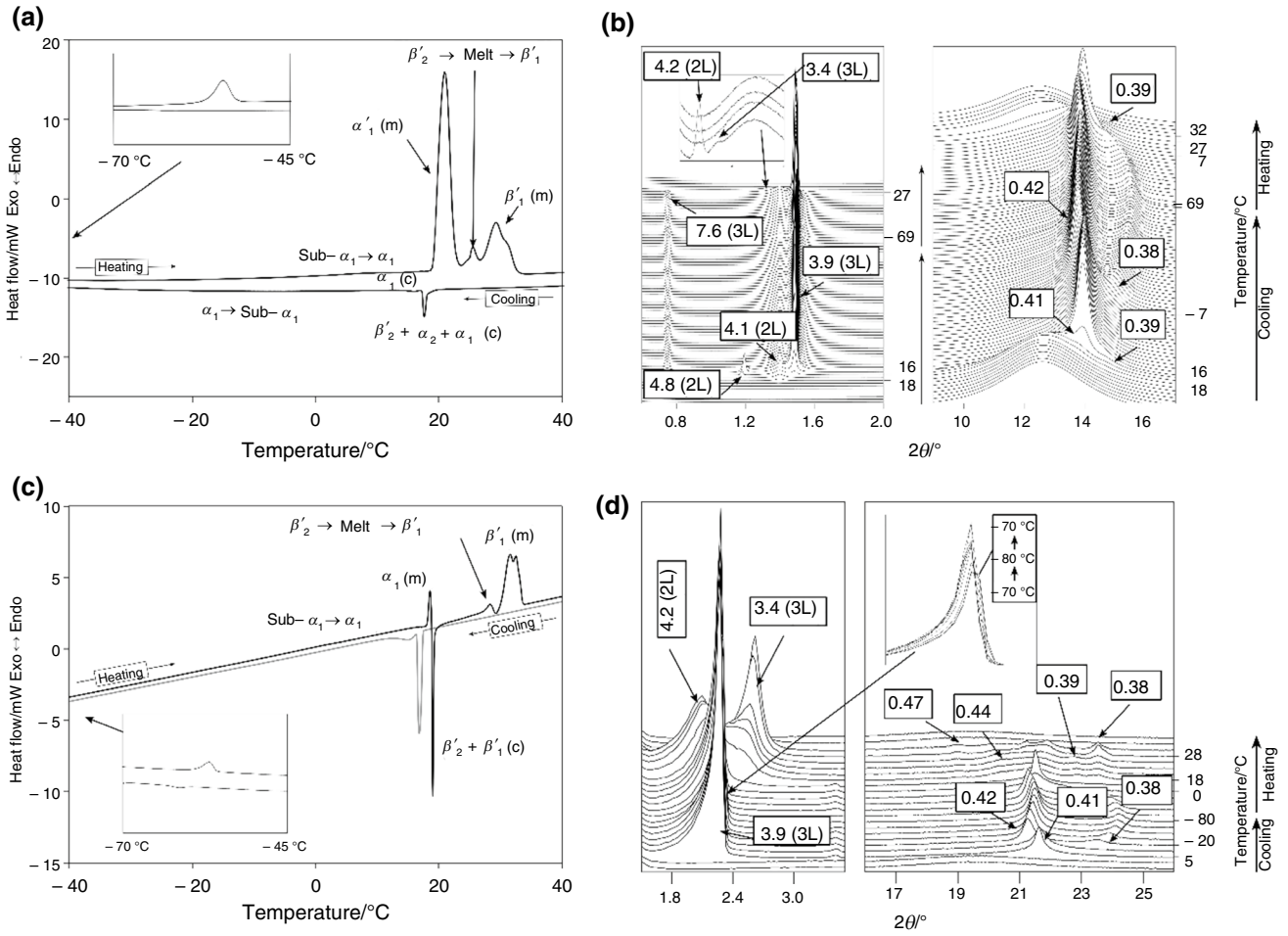

Fig. 4 DSC and XRD data of PPO heated at **A, B** 15 °C min^{-1} and **C, D** 0.5 °C min^{-1} after previous cooling at 0.5 °C min^{-1}. (c): crystallization; (m): melting. *d*-spacing values are given in nm

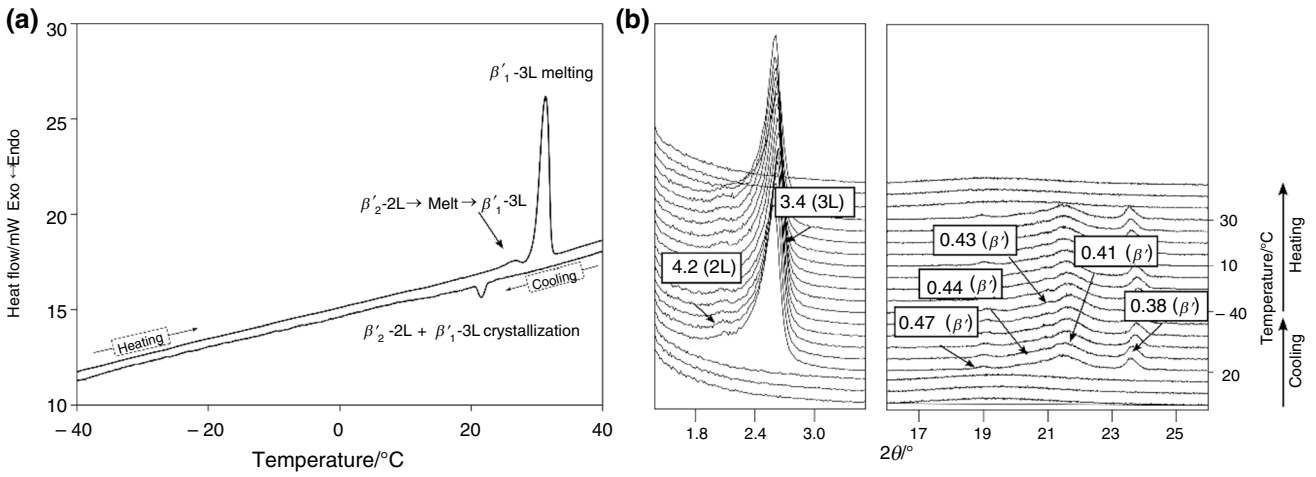

Fig. 5 DSC curves **A** and SR-XRD patterns **B** of PPO cooled at 0.1 °C min^{-1} and subsequently heated at 2 °C min^{-1}. (c): crystallization; (m): melting. *d*-spacing values are given in nm

may have been favored by the presence of some β'_2-2L crystals from the preceding cooling process. In contrast with PPO cooled at higher rates, this also eased the crystallization of β'_1-3L from the β'_2-2L melt during the heating treatment. The latter was confirmed by SR-XRD data through the weak short-life SR-SAXD signal at 3.4 nm occurring when reaching 27 °C (Fig. 4B), and by DSC through the final melting peak detected at about 30 °C. In agreement with this, PPO heated at lower rates showed melt-mediated α_1-3L → β'_2-2L and β'_2-2L → β'_1-3L transformations before complete melting (see experimental data of PPO reheated at 0.5 °C in Fig. 4C and D), respectively. One may notice that, at both heating rates, the melting of β'_1-3L led to two convoluted endothermic peaks in the DSC curves but no evidence of the presence of diverse polymorphs could be extracted from SR-XRD data. This behavior could arise from the racemic nature of the PPO used in this study. According to previous work, when S-OPP and R-PPO are mixed at an equimolecular composition, not all PPO molecules contribute to the formation of a racemic compound during crystallization, but some remain packed with their equivalent enantiomer [18]. Thus, the complex endothermic event observed in this work could be due to the successive melting of β'-3L of the racemic compound and pure enantiomers.

The polymorphic transformation behavior of PPO heated at 2 and 0.5 °C min^{-1} after cooling at 0.1 °C min^{-1} was in agreement with that of PPO previously cooled at different rates (see Figs. 5 and S1). As expected, the crystallization of more stable β'_2-2L and β'_1-3L forms during cooling reduced the number of polymorphic phenomenon when heating. Metastable β'_2-2L crystals melted first, which yield the weak endothermic signal ($\Delta H = 4$ J g^{-1}) detected at T_{onset} of ~ 25 °C in the heating curve. Then, β'_1-3L was formed and melted soon after at around 28 °C.

Microscopy study during cooling and reheating treatments

The same cooling treatments applied by DSC and XRD techniques were followed by TOPLM to analyze their effect on the crystal shape and morphology of PPO. Figure 6 depicts the optical micrographs obtained at the end of crystallization after cooling at different rates of 15, 2, 0.5 and 0.1 °C min^{-1}.

When rapidly cooled at 15 °C min^{-1} (Fig. 6A), a vast mass of small needle-shaped crystals developed. Fat crystals tend to grow radially from the nucleation site forming spherulitic structures but the microstructure observed is not unexpected in fat systems subjected to fast cooling processes [23]. In fact, these individual fibers or needles are the primary elements of spherulites [24], but the processing conditions lead them to grow separately and adopt random orientations. When more time was provided to the sample to crystallize, PPO molecules arranged in the form of spherulites showing birefringent Maltese crosses, and they varied in size and shape at the different cooling rates employed. At 2 °C min^{-1} (Fig. 6B), small irregular structures with 10–25 µm diameter predominated in the crystallized mass. As to the PPO spherulites obtained at 0.5 °C min^{-1} (~ 30 µm), branched structures could be clearly discerned under the microscope (Fig. 6C). This could be related to

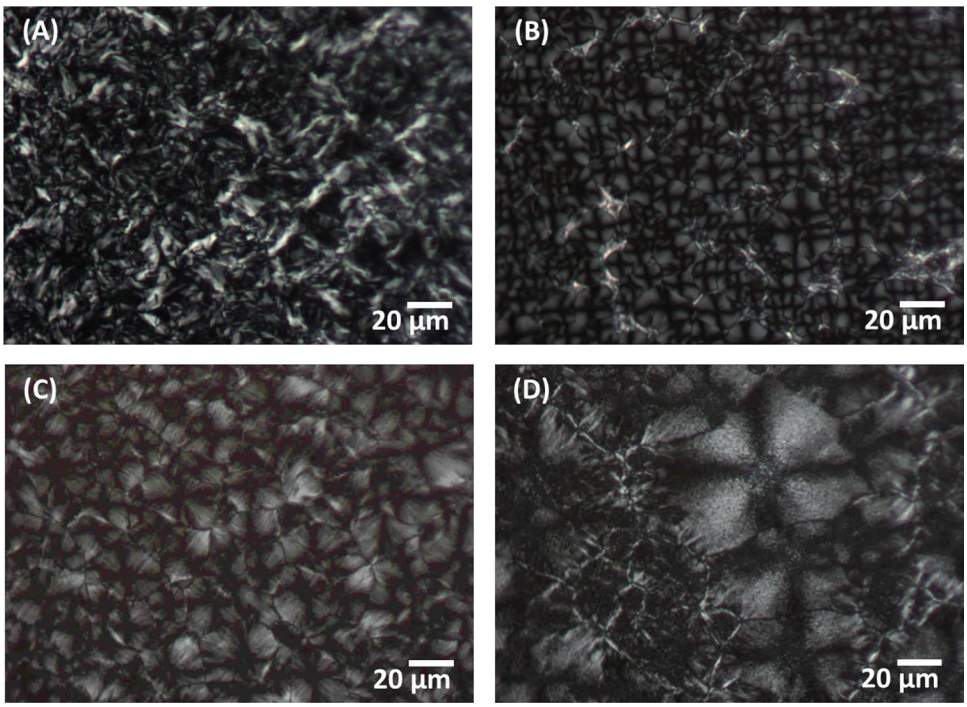

Fig. 6 Optical micrographs obtained after the crystallization of PPO cooled at **A** 15 °C min^{-1}, **B** 2 °C min^{-1}, **C** 0.5 °C min^{-1}, and **D** 0.1 °C min^{-1}

the occurrence of β'_2-2L form during the cooling process, as indicated by SR-XRD experiments (Fig. 4B). In this connection, previous microscopic studies on PPP have shown that α-2L crystals are usually in the form of bright spherulites, whereas β'-2L crystals may arise as densely packed structures showing branches or fibers running outward radially [25, 26]. Finally, as expected from the lower degree of supercooling, the PPO sample cooled at the lowest rate of 0.1 °C min^{-1} showed a much lower number of spherulitic structures exhibiting higher dimensions (up to 80 µm) and a grainy texture (Fig. 4D).

During subsequent heating treatments at high rates, it was not possible to discern the different polymorphic transitions by TOPLM. However, the combination of low cooling and heating rates made possible to visualize the microstructural changes occurring in PPO during transitions in which forms of higher stability were involved. The optical micrographs obtained when heating PPO at 0.5 °C min^{-1} after cooling at the same rate are depicted in Fig. 7.

During slow heating, the β'_2-2L to β'_1-3L transition was monitored through the increase in brightness of the spherulitic clusters of PPO between 25 °C and 29 °C. At these temperatures, PPO was in the form of β'_2-2L and β'_1-3L crystals, respectively, according to lab-scale XRD data (Fig. 4D). Furthermore, the size of spherulites slightly decreased and the edges became noticeably sharper at the higher temperature. This was visual evidence of a noteworthy increase in the density of molecular packing undergone by PPO molecules when arranged in the most stable polymorph.

Discussion

The polymorphic behavior for PPO during the application of dynamic thermal treatments is summarized in Fig. 8.

As shown, at fast and intermediate cooling processes, the occurrence of α form was strongly favored. Moreover, SR-XRD data suggested that the initial formation of α_2-2L might be a necessary condition for the development of α_1-3L. A low cooling rate of 0.5 °C min^{-1} led to the occurrence of some β'_2-2L, but short-life α_2-2L crystals still formed and α_1-3L ones predominated at the end of the process. Only when the rate was decreased to 0.1 °C min^{-1}, the formation

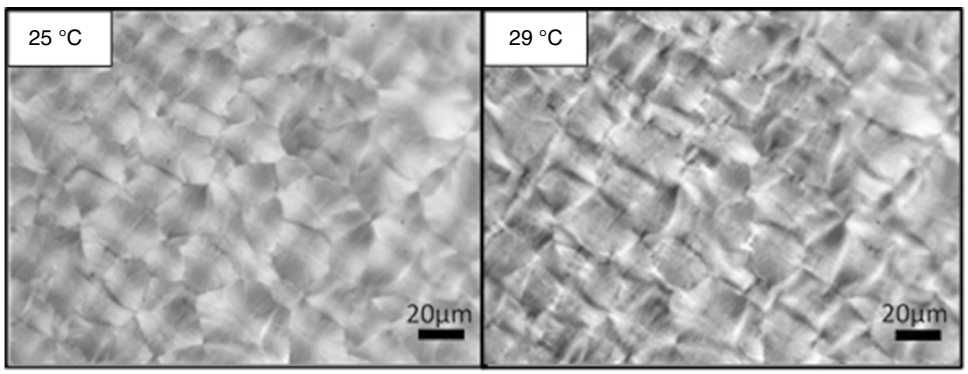

Fig. 7 Microstructural changes of PPO during the $\beta'_2 \rightarrow \beta'_1$ transformation at a heating rate of 0.5 °C min^{-1}

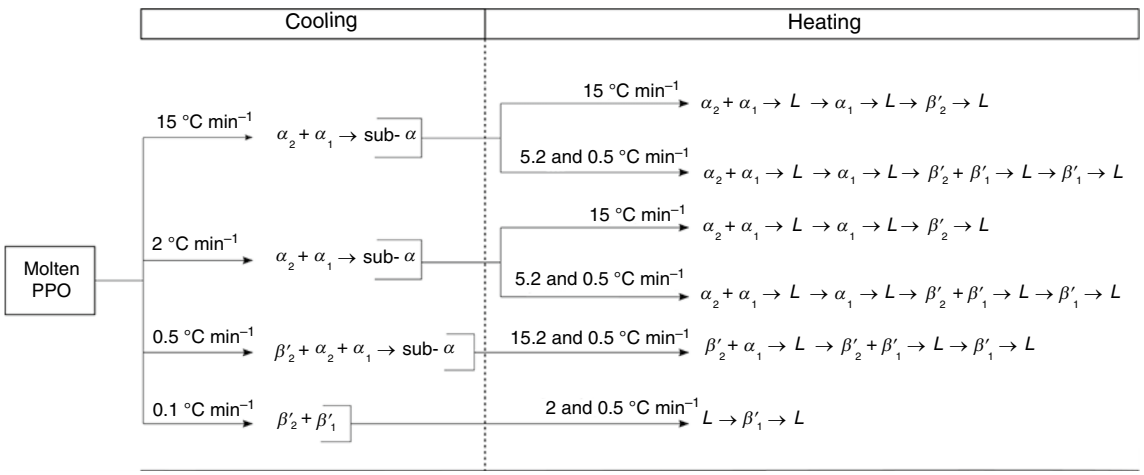

Fig. 8 Polymorphic crystallization and transformation pathways shown by PPO under different cooling and heating conditions. L: liquid

of α forms was avoided and β'_1-3L crystals, together with those of β'_2-2L form, were obtained.

This predominance of more stable forms when decreasing the rates of cooling and heating is clearly in accordance with the enthalpy values associated to the melting of the different polymorphs, which are shown in Tables S1 and S2. As an example, when decreasing the heating rate, the enthalpy for the melting of β'_1 increased at the expense of that of α_1, due to higher amounts of the more stable form obtained. This may be observed, for instance, for conditions of cooling at 15 °C min^{-1} when comparing the corresponding enthalpies detected during the heating steps at 5, 2 and 0.5 °C min^{-1}; for cooling at 2 °C min^{-1} and heating at 5, 2 and 0.5 °C min^{-1}; or for cooling at 0.5 °C min^{-1} and heating at 15, 2 and 0.5 °C min^{-1}.

During the microscopic study of PPO, no specific crystal morphologies could be associated to each polymorphic form. The main difference observed during cooling treatments remained in the increasing size of the spherulitic structures formed at decreasing rates.

The behavior of PPO is explained by the polymorphic-dependent crystallization of TAGs under varying temperature conditions. The formation of a specific form rather than other is determined by its rate of nucleation, which in turn is ruled by the activation free energy of nucleation (ΔG_n) and the degree of supercooling (ΔT) or the difference between the melting temperature and the crystallization temperature [10]. ΔG_n decreases from the most stable β to the least stable α form, from which one may expect that the crystallization of more stable forms is favored before less stable ones due to a higher driving force [27]. However, increasing the degree of supercooling by applying fast cooling treatments reduces the crystallization temperature, which leads to the crystallization of less stable crystals.

We may compare our results with those reported in the literature for other saturated–unsaturated mixed-acid TAGs crystallized under non-isothermal conditions. The polymorphic forms characteristic of some of these TAGs is included in Table 2 [15, 28, 29].

In essence, we could conclude a higher tendency of PPO to crystallize in α form even at low cooling rates. For example, Bayés-García and co-authors thoroughly investigated the crystallization and transformation behavior of symmetric and asymmetric TAGs including palmitic and oleic acids. The authors observed that α-2L crystals of OPO occurred when this TAG was cooled at 15 °C min^{-1}, whereas intermediate and low cooling rates (2 and 0.5 °C min^{-1}) favored the crystallization of more stable β' and β forms [13]. In POO, characteristic TAG of the low-melting fraction of palm oil, α crystals predominated when cooling at 15 or 2 °C min^{-1}, but decreasing the rate to 0.5 °C min^{-1} resulted in the concurrent crystallization of its β'_2 and β'_1 forms [15]. As for POP, γ form was favored before the least stable α when cooling

Table 2 Main polymorphic forms and chain-length structure of TAGs with varying fatty acid composition, degree of unsaturation, and symmetry [15, 28, 29]

TAG	Polymorphs and chain-length structure
POP	α-2L, γ-3L, β'-2L, δ-3L, β-3L
OPO	α-2L, β'-2L, β-3L
POO	sub-α-2L, α-2L, KLC, β'-3L
POL	sub-α-2L, α-2L, β'-3L
SOS	α-2L, γ-3L, β'-3L, β-3L
SOO	sub-α-2L, α-2L, KLC, β'-3L
OOO	α-2L, β'-2L, β-2L
OOL	α-2L, β'-2L
SLS	α-2L, γ-3L

O: oleic acid; L: linoleic acid; P: palmitic acid; S: stearic acid

KLC: kinetic liquid crystal

rates from 1 °C min^{-1} and below were applied [14]. In SLS (with L being linoleic acid), γ was obtained from the melt at a faster cooling rate of 5 °C min^{-1} [28]. Finally, cooling treatments at 1 °C min^{-1} and below promoted the occurrence of β' and hindered that of α and γ in SOS [12]. The favored crystallization of PPO in α form and, concretely, α_2-2L, could be in part related with the fact that molten lipids exhibit some degree of molecular order even at temperatures far above their melting point [30]. The strength of dipole–dipole interactions between carbonyl groups (C = O) of the glycerol backbones and Van der Waals forces between aliphatic chains of TAGs in the molten state may be enough to enable molecular aggregation in lamellar-like structures [31]. Moreover, it has been already suggested that the first occurring α forms of monounsaturated TAGs such as SOS, SLnS (with Ln being linolenic acid), and PPO consist of transient mesophases inheriting the structural arrangement of smectic-A liquid crystalline phases (with hexagonal in-plane order) [20, 32–34]. The relatively simple polymorphic properties of PPO with respect to other monounsaturated TAGs also influenced the more prevalent α forms obtained during crystallization. The lateral packing of PPO molecules may lead to either α and β' forms. In between these, TAGs with different symmetry, such as POP, exhibit intermediate γ and/or δ forms. As stated before, the polymorphic-dependent crystallization is influenced by the activation free energy of nucleation and the degree of supercooling. In addition, we know that the energy barrier to overcome for the crystallization of a specific form becomes higher as the density of molecular packing increases. Therefore, it is comprehensible the much lower reduction in the degree of supercooling (lower cooling rates) needed to induce a change of subcell arrangement in PPO. In addition, we should also consider the racemic nature of the PPO used in this study on the crystallization behavior observed. Mizobe et al. demonstrated

that, contrary to the racemic mixture, pure R(S)-PPO enantiomers pack in β' during cooling processes at 2 °C min^{-1} and α crystals only occur in very fast cooling processes [18].

As to the transformation behavior of PPO during reheating treatments, the higher time for polymorphic transitions to occur provided by slow heating led to a higher number and better-defined polymorphic transitions in the heating curves obtained at 2 and 0.5 °C min^{-1} than at 15 °C min^{-1} (see Fig. 1). In addition to the stronger DSC signals attributed to melting and recrystallization events, the promoted transition to more stable form was recognized by SR-XRD through a remarkable increase in the intensity of β'_2-2L and β'_1-3L reflections. However, the different heating conditions applied did not influence the overall transformation pathways and the sequence of polymorphic transitions (see Fig. 8). PPO polymorphs obtained during crystallization at different rates, when reheating, transited to the next one in order of increasing stability (sub-$\alpha \rightarrow \alpha_2$-2L$\rightarrow \alpha_1$-3L$\rightarrow \beta'_2$-2L$\rightarrow \beta'_1$-3L) via melt-mediation. This contrasts with the complex transformation behavior revealed by saturated–unsaturated mixed-acid TAGs like SOO, POO, and POL. In these, the α-2L form always transformed into the most stable β'-3L form via melt-mediation at high heating rates (15 °C min^{-1}), whereas reducing the rate (2–0.5 °C min^{-1}) led to transformations through the solid-state or via kinetic liquid crystal phases [15]. As to POP, the solid-state transformation of α-2L into the following more stable γ-3L form was only promoted when rates below 2 °C min^{-1} were applied [14]. Interestingly, α-2L transformed directly into β'-2L through the melt during fast heating at 15 °C min^{-1}. Similar behavior was determined in the γ-3L$\rightarrow\beta$-3L transformation, which only at the very low rate of 0.1 °C min^{-1} occurred in the solid-state through the intermediate δ-3L. These varying polymorphic transformation pathways followed by TAGs are explained through the Gibbs free energy of activation involved in the structural changes during phase transitions ($\Delta G^{\#}$) (changes in lamellar and subcell arrangements) and the induction times (τ) required for the different transformations to occur (simple melting, via melt-mediation, through the solid-state, or via kinetic liquid crystalline phases). It is assumed that the energy barrier for a melt-mediated transformation to occur is lower than that of a solid-state transformation [35]. In addition, the time available for a transformation to occur increases as the heating rate is decreased. Thus, solid-state transformations are usually promoted at low cooling rates, whereas high heating rates usually favor melt-mediated transformations (with lower $\Delta G^{\#}$ and τ).

The intrinsic structural properties of PPO may also have a key role in the transformation behavior observed. In contrast with the β'_2-2L$\rightarrow$melt$\rightarrow\beta'_1$-3L transformation of PPO at heating rates from 0.5 to 15 °C min^{-1}, solid β'_2-3L$\rightarrow\beta'_1$-3L transitions of SOO, POL, and POO took place when heated at the same rates [15]. A higher degree of structural changes occurs when a transformation implies a conversion from a double to a triple chain-length structure (or vice versa) than in transformations that do not require changes in the longitudinal packing. Thus, $\Delta G^{\#}$ is expected to be higher when starting and final polymorphs differ in chain-length structure. This relates to the favored melt-mediated transformation of PPO, whose polymorphs in order of increasing stability show sequential double and triple chain-length structures. The effect of palmitic acid at two *sn*- positions of the glycerol group of PPO may also be considered. The lower flexibility of the chain packing associated with the straight zigzag configuration of saturated fatty acids [36] may lead to greater $\Delta G^{\#}$ values in PPO than in TAGs with a higher degree of unsaturation. This would relate to the also hindered solid-state transitions reported for the symmetric TAG POP even at a the very low heating rate of 0.1 °C min^{-1} [14].

Conclusions

The results obtained during the polymorphic study of PPO subjected to dynamic thermal treatments at varying rates were in great agreement with previous data on common unsaturated TAGs contained in edible fats and oils. At decreasing rates, more stable forms crystallize during cooling and higher amounts of specific crystalline phases are obtained during the transformations occurring on heating. However, in comparison with other TAGs, PPO showed a lower variability in the polymorphic occurrence during the crystallization at varying cooling rates, which mainly led to the formation of low-stable α crystals except at very low cooling rates. In addition, PPO showed a steady sequence of polymorphic transformations mainly via melt-mediation during the different heating treatments applied. The characteristic behavior observed in PPO was probably determined by structural factors, such as the molecular symmetry and the oleic acid content. Lower cooling and heating rates than those applied in the present study may be needed to induce remarkable changes in the polymorphic occurrence and the transformation pathways of this TAG during thermal treatments. The polymorphic properties here reported might be considered for a better understanding of the crystallization processes occurring during the manufacture of solid and semi-solid food products based on PPO-rich lipids, such as olive oil hard fractions.

Supplementary Information The online version contains supplementary material available at https://doi.org/10.1007/s10973-024-13844-8.

Acknowledgements The authors acknowledge the Generalitat de Catalunya through project 2021 SGR 00262, and the financial support of Grant PID2019-107032RB-I00 funded by MCIN/AEI/https://doi.org/10.13039/501100011033/. Funding from the ALBA synchrotron

facility is also gratefully acknowledged. SR-XRD experiments were performed with the approval of the ALBA Scientific Advisory Committee (proposal 2019023268). The authors thank Dr. Marc Malfois, responsible for the BL11-NCD-SWEET at ALBA, for his assistance.

Authors' contributions All authors contributed to the experimental design. Experiments, data acquisition and analyses were carried out by J.M. The original draft of the manuscript was prepared by J.M. Funding acquisition was done by L.B.-G. and T.C. Manuscript review was performed by L.B. and T.C.

Funding Open Access funding provided thanks to the CRUE-CSIC agreement with Springer Nature.

Declarations

Conflict of interest The authors have no competing interests to declare that are relevant to the content of this article.

References

1. Larsson K, Quinn P, Sato K, Tiberg F. Lipids: structure, physical properties and functionality. Bridgewater, UK: The Oily Press; 2006.
2. DeMan JM, DeMan L. Polymorphism and texture of fats. In: Widlak H, Hartel R, Narine S, editors. Crystallization and solidification properties of lipids. Champain: AOCS Press; 2001. p. 225–35.
3. Ghotra BS, Dyal SD, Narine SS. Lipid shortenings: a review. Food Res Int. 2002;35:1015–48.
4. Mazzanti G, Guthrie S, Sirota EB, Marangoni A, Idziak SHJ. Orientation and phase transitions of fat crystals under shear. Cryst Growth Des. 2003;3:721–5.
5. Ramel PR, Campos R, Marangoni AG. Effects of shear and cooling rate on the crystallization behavior and structure of cocoa butter: shear applied during the early stages of nucleation. Cryst Growth Des. 2018;18:1002–11.
6. Sonwai S, Mackley MR. The effect of shear on the crystallization of cocoa butter. J Am Oil Chem Soc. 2006;83:583–96.
7. Da Silva TLT, Martini S. Crystallization of interesterified soybean oil using a scraped surface heat exchanger with high intensity ultrasound. J Food Eng. 2019;263:341–7.
8. Sonwai S, Ornla-ied P, Martini S, Hondoh H, Ueno S. High-intensity ultrasound-induced crystallization of mango kernel fat. J Am Oil Chem Soc. 2021;98:43–52.
9. Ueno S, Ristic RI, Higaki K, Sato K. *In situ* studies of ultrasound-stimulated fat crystallization using synchrotron radiation. J Phys Chem B. 2003;107:4927–35.
10. Sato K, Kuroda T. Kinetics of melt crystallization and transformation of tripalmitin polymorphs. J Am Oil Chem Soc. 1987;64:124–7.
11. Koyano T, Hachiya I, Arishimo T, Sato K, Sagi N. Polymorphism of POP and SOS. II. Kinetics of melt crystallization. J Am Oil Chem Soc. 1989;66:675–9.
12. Baker MR, Bouzidi L, Garti N, Narine SS. Multi-length-scale elucidation of kinetic and symmetry effects on the behavior of stearic and oleic TAG. I. SOS and SSO. J Am Oil Chem Soc. 2014;91:559–70.
13. Bayés-García L, Calvet T, Cuevas-Diarte MA, Ueno S, Sato K. In situ synchrotron radiation X-ray diffraction study of crystallization kinetics of polymorphs of 1,3-dioleoyl-2-palmitoyl glycerol (OPO). CrystEngComm. 2011;13:3592–9.
14. Bayés-García L, Calvet T, Cuevas-Diarte MA, Ueno S, Sato K. *In situ* observation of transformation pathways of polymorphic forms of 1,3-dipalmitoyl-2-oleoyl glycerol (POP) examined with synchrotron radiation X-ray diffraction and DSC. CrystEngComm. 2013;15:302–14.
15. Bayés-García L, Calvet T, Cuevas-Diarte MA, Ueno S. In situ crystallization and transformation kinetics of polymorphic forms of saturated-unsaturated-unsaturated triacylglycerols: 1-palmitoyl-2,3-dioleoyl glycerol, 1-stearoyl-2,3-dioleoyl glycerol, and 1-palmitoyl-2-oleoyl-3-linoleoyl glycerol. Food Res Int. 2016;85:244–58.
16. Noorzyanna Y, Marikkar N, Mustafa S, Mat SM. Composition and thermal analysis of ternary mixtures of avocado fat:palm stearin:cocoa butter (Avo:PS:CB). Int J Food Prop. 2017;20:465–74.
17. Bayés-García L, Calvet T. Deconstructing extra virgin olive oil through fractionation processes. Food Res Int. 2022;162:111945.
18. Mizobe H, Tanaka T, Hatakeyama N, Nagai T, Ichioka K, Hondoh H, Ueno S, Sato K. Structures and binary mixing characteristics of enantiomers of 1-oleoyl-2,3-dipalmitoyl-sn-glycerol (S-OPP) and 1,2-dipalmitoyl-3-oleoyl-sn-glycerol (R-PPO). J Am Oil Chem Soc. 2013;90:1809–17.
19. PerkinElmer (1982) Instructions Model DSC-4. Norwalk: PerinElmer
20. Mykhaylyk OO, Smith KW, Martin CM, Ryan AJ. Structural models of metastable phases occurring during the crystallization process of saturated/unsaturated triacylglycerols. J Appl Crystallogr. 2007;40:297–302.
21. Norris R (1977) The physical properties of triacylglcyerols in relation to milkfat. Massey University
22. Taguchi K, Toda A, Hondoh H, Ueno S, Sato K. Kinetic study on alpha-form crystallization of mixed-acid triacylglycerols POP, PPO, and their mixture. Molecules. 2021;26:220.
23. Yang D, Hrymak AN. Crystal morphology of hydrogenated castor oil in the crystallization of oil-in-water emulsions: Part I. Effect of temperature. Ind Eng Chem Res. 2011;50:11585–93.
24. Rousset P. Modeling crystallization kinetics of triacylglycerols. In: Marangoni AG, Narine SS, editors. Physical properties of lipids. New York: Marcel Dekker; 2002. p. 1–36.
25. Kellens M, Meeussen W, Reynaers H. Study of the polymorphism and the crystallization kinetics of tripalmitin: a microscopic approach. J Am Oil Chem Soc. 1992;69:906–11.
26. Da Silva RC, De Martini Soares FAS, Maruyama JM, Dagostinho NR, Silva YA, Ract JNR, Gioielli LA. Microscopic approach of the crystallization of tripalmitin and tristearin by microscopy. Chem Phys Lipids. 2016;198:1–9.
27. Himawan C, Starov VM, Stapley AGF. Thermodynamic and kinetic aspects of fat crystallization. Adv Colloid Interface Sci. 2006;122:3–33.
28. Takeuchi M, Ueno S, Yano J, Flöter E, Sato K. Polymorphic transformation of 1,3-distearoyl-sn-2-linoleoyl-glycerol. J Am Oil Chem Soc. 2000;77:1243–50.

29. Sato K, Arishima T, Wang Z, Okima K, Sagi N, Mori H. Polymorphism of POP and SOS. I. Occurrence and polymorphic transformation. J Am Oil Chem Soc. 1989;66:664–74.
30. Hernqvist L. On the structure of triglycerides in the liquid state and fat crystallization. Fette, Seifen, Anstrichm. 1984;86:297–300.
31. Hondoh H, Ueno S, Sato K. Fundamental aspects of crystallization of lipids. In: Sato K, editor. Crystallization of lipids fundamentals and applications in food, cosmetics and pharmaceuticals. Wiley-Blackwell: Hoboken; 2018. p. 105–42.
32. Mykhaylyk OO, Castelletto V, Hamley IW, Povey MJW. Structure and transformation of low-temperature phases of 1,3-distearoyl-2-oleoyl glycerol. Eur J Lipid Sci Technol. 2004;106:319–24.
33. Mykhaylyk OO, Martin CM. Effect of unsaturated acyl chains on structural transformations in triacylglycerols. Eur J Lipid Sci Technol. 2009;111:227–35.
34. Seddon JM. Structural studies of liquid crystals by x-ray diffraction. In: Demus D, Goodby J, Gray GW, Spiess H-W, Vill V, editors. Handbook of liquid crystals. Weinheim: Wiley-VCH; 1998. p. 635–79.
35. Sato K, Ueno S. Crystallization, transformation and microstructures of polymorphic fats in colloidal dispersion states. Curr Opin Colloid Interface Sci. 2011;16:384–90.
36. Small DM. Lateral chain packing in lipids and membranes. J Lipid Res. 1984;25:1490–500.